Supporting Information

Khan et al. 10.1073/pnas.1214533110

SI Results

Long-Range Coherence. Movie S1 corresponds to Fig. 2, illustrating the long-range coherence between the fusiform face area (FFA) and the rest of the cortex. Because coherence was computed using a sliding time window, we were able to see how it changes in time. Whereas Fig. 2 provides static snapshots of the results, Movie S1 provides a dynamic picture of Z-Coherence in each group as it evolves in time relative to stimulus onset.

Local Functional Connectivity. Phase-amplitude coupling (PAC) for two participants, one from each group, is illustrated in Fig. S1*A*. Fig S1*B* confirms that the observed PAC differences do not arise from differences in intertrial coherence (ITC) (1). This latter result is also supported by other studies (2). Fig. S2 shows whole-cortex PAC data for the houses condition and emotional faces condition, and Fig. S3 provides additional views of the normalized PAC value (Z-PAC) data presented in Fig. 3*C* (PAC for emotional faces condition normalized by PAC for the houses condition).

Correlation Between Local and Long-Range Functional Connectivity. Fig. S4 shows the correlation between Z-PAC and Z-Coherence within each group, and thus complements Fig. 4.

Functional Connectivity and Autism Spectrum Disorders Severity and Diagnosis. Movie S2 is a rotating version of the five dimensions (Z-PAC, Z-Coherence on three axes, and probability; Fig. 5*B*) projected onto three dimensions. Quadratic discriminant analysis (QDA) is a probabilistic classifier, meaning each data point is assigned a probability of belonging to a group. Looking at the individual data, it is clear that all but one participant were assigned the correct probability, well above or below 50%, in accordance with their diagnosis. Only one participant with autism spectrum disorders (ASD) was assigned a roughly 50% probability of belonging to the ASD group, meaning the model could not classify that participant correctly. In other words, a hypercurve can be drawn that would completely separate the groups except for one participant. This result is striking because the vast majority of studies looking for ASD biomarkers find group differences in the means but large overlaps between groups when individual data are considered (e.g., ref. 3).

Receiver Operating Characteristic Curves for Different Statistical Classifiers. Fig. S4 shows the receiver operating characteristic (ROC) curves for the QDA classifier using different subsets of the data, as well as the ROC curve for a linear discriminant analysis (LDA) classifier. The performance of the two classifiers was equivalent (details are provided in the legend for Fig. S4).

No Group Differences in the Induced Response. Fig. S5 shows the induced response in each group, condition, and region of interest (details of how the induced response was computed are provided in the legend for Fig. S5).

SI Materials and Methods

Participants. Participants were 17 adolescent and young adult males diagnosed with ASD and 20 age-matched typically developing (TD) males. Data were obtained for 5 additional participants (4 diagnosed with ASD and 1 diagnosed as TD) who were excluded from our analysis due to excessive movement or poor head position localization. Two of our participants (both TD) with initially poor data quality returned for a second, successful MEG session, and these data are included in our analysis.

Participants were recruited through community sources. Participants with ASD were recruited for having a prior diagnosis of ASD and were required to meet a cutoff of >15 on the Social Communication Questionnaire (SCQ), Lifetime Version. Individuals with autism-related medical conditions (e.g., fragile X syndrome, tuberous sclerosis) and other known risk factors (e.g., premature birth) were not included in this study. Participants with ASD were subsequently assessed with either module 3 ($n = 3$) or module 4 ($n = 14$) of the Autism Diagnostic Observation Schedule (ADOS) (4), which was administered by trained research personnel who had previously established interrater reliability. All participants met ADOS classificatory criteria for autism ($n = 7$) or ASD ($n = 9$), with the exception of one participant who exceeded the ADOS autism cutoff for social symptoms but had a score one below the cutoff for communication symptoms. This individual was rated 27 on the SCQ, and was confirmed by clinical impression to meet diagnostic criteria of the *Diagnostic and Statistical Manual of Mental Disorders*, fourth edition, for pervasive developmental disorder.

All TD participants were scored below threshold on the SCQ and were confirmed to be free of any neurological or psychiatric conditions, as well as free of substance use for the past 6 mo, via parent and self-report and clinical observation. The ASD and TD groups did not differ in verbal or nonverbal intelligence quotient (IQ), as measured with the Kaufman Brief Intelligence Test, second edition (5). Handedness information was collected using the Dean Questionnaire (6) for 34 participants and was self-reported for the remaining 3 participants. Each group had 1 ambidextrous participant, and the ASD group had 2 left-handed participants. The rest of the participants were right-handed. Participant data are shown in Table S1.

Experimental Paradigm and Task. The paradigm presented in the magnetoencephalography (MEG) studies consisted of houses and neutral, fearful, and angry faces (Fig. S6). Each stimulus was displayed for 1 s, separated by 1 s of fixation cross baseline (fixation on a cross at the center of the screen). Eight stimuli of the same condition were presented consecutively. The paradigm was presented in three consecutive runs. Each run lasted 3 min and consisted of eight blocks, two of each condition, presented in random order within the run, followed by a short break (1–2 min). To ensure attention, participants were asked to press a button when the same face appeared twice in succession. This was a rare (1/8) occurrence, and all participants performed at ceiling level on the task. We were not concerned about motor-preparation artifacts from trials involving a button press, because our analysis was always time-locked to stimulus onset. Therefore, the non–time-locked effects from the 16% of trials associated with a motor response would average out to a level no greater than the noise inherent in the data.

The face stimuli were collected from three databases: Karolinska Directed Emotional Faces (KDEF) (7), NimStim Face Stimulus Set, and Gur (8). The houses stimuli were obtained from the Kanwisher Laboratory database at Massachusetts Institute of Technology. All stimuli were homogenized using an oval black mask. The sequence of stimuli was generated and presented using the psychophysics toolbox (9, 10), and presented with a projector through an opening in the wall onto a back-projection screen placed 100 cm in front of the participant inside a magnetically shielded room.

Structural MRI Data Acquisition and Processing. T1-weighted, high-resolution, magnetization-prepared rapid gradient echo structural images were acquired on a 3.0-T Siemens Trio whole-body

magnetic resonance scanner (Siemens Medical Systems) using a 32-channel head coil. The images were acquired with a 1-mm × 1-mm in-plane resolution, 1.3-mm slice thickness with no gaps, and a repetition time/time following inversion pulse/echo time/flip angle of 2,530 ms/1,100 ms/3.39 ms/7°. Cortical reconstructions and parcellations for each subject were generated using FreeSurfer (11, 12). After correcting for topological defects, cortical surfaces were triangulated with dense meshes with ∼130,000 vertices in each hemisphere. To expose the sulci in the visualization of cortical data, we used the inflated surfaces provided by FreeSurfer (11).

MEG Data Acquisition and Preprocessing. ***Acquisition.*** The MEG data were acquired inside a magnetically shielded room (IMEDCO) using a whole-head Elekta Neuromag VectorView system composed of 306 sensors arranged in 102 triplets of two orthogonal planar gradiometers and one magnetometer. The signals were filtered between 0.1 Hz and 200 Hz and sampled at 600 Hz. The position and orientation of the head with respect to the MEG sensor array were recorded continuously throughout the session (at 200-ms intervals) during each trial with the help of four head position indicator (HPI) coils (13). These continuous head position data were later used to apply movement correction to each individual participant. To allow coregistration of the MEG and MRI data, the locations of three fiduciary points (nasion and auricular points) that define a head-based coordinate system, a set of points from the head surface, and the sites of the four HPI coils were digitized using a Fastrak digitizer (Polhemus) integrated with the VectorView system. ECG and electrooculogram (EOG) signals were recorded simultaneously to identify epochs containing heartbeats as well as vertical and horizontal eye movement and blink artifacts. During data acquisition, online averages were computed from artifact-free trials to monitor data quality in real time. All off-line analysis was based on the saved continuous raw data. In addition, 5 min of data from the room void of a subject were recorded before each experimental session for noise estimation purposes.

Noise suppression and motion correction. The data were spatially filtered using the signal space separation (SSS) method (14, 15) with Elekta Neuromag Maxfilter software to suppress noise generated by sources outside the brain. This SSS procedure also corrects for head motion between runs as well as within each run, using the continuous head position data described in the previous section. The heartbeats were identified using in-house MATLAB code modified from QRS detector in BioSig (16). Subsequently, a signal-space projection operator was computed separately for magnetometers and gradiometers using the Singular Value Decomposition (SVD) of the concatenated data segments containing the QRS complexes. Data were also low-pass filtered at 145 Hz to eliminate the HPI coil excitation signals.

Epoching. The data were epoched into single trials lasting 2 s, from 800 ms before stimulus onset to 1,200 ms following it. A total of 48 trials were collected for each of the four conditions. Epochs were rejected if the peak-to-peak amplitude during the epoch exceeded 150 μV, 1,000 fT, and 3,000 fT/cm in any of the EOG, magnetometer, and gradiometer channels, respectively. This resulted in the loss of 2–8 trials per participant per condition. To maintain a constant signal-to-noise ratio across conditions and participants, we fixed the number of trials per condition per participant at 40, the minimum number of accepted trials that we had for each condition and participant. For conditions and participants having more than 40 good trials, we selected 40 trials randomly from the available trials. There were no group differences in overall quality of the data, and the number of good (unrejected) trials per condition was not significantly different between groups or across conditions. For each participant, the same set of trials was used for all the analyses (delineation of FFA, coherence, and PAC).

Eye tracking. Prior research has shown that individuals with ASD tend to look away from faces or away from the eye region of the face (17), which can have an impact on responses in the FFA (18, 19). It has also been shown that individuals with ASD can be biased to look at the eye region by using a fixation point at the correct location, as we did, and that in such cases, FFA activation normalizes in individuals with ASD as a function of the amount of time spent looking at the eye region (20–22). To verify fixation, we recorded participants' eye movements using two EOG electrodes placed above and below the left eye to track vertical eye movements and near the temporal end of each eye to track horizontal eye movements. Although EOG electrodes do not record absolute eye gaze direction, they record changes in eye gaze direction in a highly reliable manner. We found that eye movements in unrejected epochs were similar across groups for all conditions. Because each trial consisted of a fixation period followed by the stimulus, this means the participants with ASD maintained their fixation throughout each trial similar to the TD participants. Although EOG tracking does not inform about absolute direction of gaze, we verified that participants with ASD fixated near the fixation point (which overlapped closely with the top of the nose) by examining the evoked responses in the FFA for each participant and group. As shown in *SI Results*, we found no significant group difference in evoked responses to faces in the FFA region, indicating that the absolute direction of fixation did not differ between groups (20–22).

Mapping MEG Data onto Cortical Space. ***Source estimation.*** The dense triangulation of the folded cortical surface provided by FreeSurfer was decimated to a grid of 10,242 dipoles per hemisphere, corresponding to a spacing of ∼3 mm between adjacent source locations. To compute the forward solution, a boundary-element model with a single compartment bounded by the inner surface of the skull was assumed (23). The watershed algorithm in FreeSurfer was used to generate the inner skull surface triangulations from the MRI scans of each participant. The current distribution was estimated using the minimum-norm estimate (MNE) by fixing the source orientation to be perpendicular to the cortex. The noise covariance matrix used to calculate the inverse operator was estimated from data acquired in the absence of a subject before each session. This approach has been validated using intracranial measurements (24). To reduce the bias of the MNEs toward superficial currents, we incorporated depth weighting by adjusting the source covariance matrix, which has been shown to result in a spatial specificity of cortical MEG data of less than 1 cm (25).

Cortical parcellations. The fusiform gyrus, anterior cingulate cortex (ACC), inferior frontal gyrus (IFG), and precuneus were identified automatically by the FreeSurfer anatomical parcellation of the cortex (11, 12).

Intersubject cortical surface registration for group analysis. The cortical surface of each participant was registered to an average cortical representation (FsAverage in FreeSurfer) by optimally aligning individual sulcal-gyral patterns (26).

Delineating the FFA. To delineate the FFA, we first identified the frontal gyrus in each participant using the individual FreeSurfer anatomical parcellation. We then aligned single trials in the houses and neutral faces conditions by latency. The latency estimation procedure is based the method of Gramfort et al. (27), and it was adapted for cortical space data. By aligning single trials so that for each participant, the latency at the peak of the response is the same for all trials, temporal jitters in single-trial brain responses could be corrected. To delineate the FFA within the frontal gyrus, we used a vertex-by-vertex statistical analysis of the peak of the evoked response to neutral faces vs. the peak of response to evoked houses. The FFA is defined as the region in the frontal gyrus that responds more strongly to faces than to houses (28). Accordingly, we identified all vertices in the frontal gyrus that responded more strongly to faces than to houses and

used cluster-based statistical analysis to eliminate spurious results and correct for multiple comparisons (Fig. S7). The resulting region comprised the FFA for that participant. The procedure was repeated for each participant, and the mean FFA size in our participants was 0.65 cm^2, in agreement with the fMRI literature. This statistical procedure yielded very high spatial specificity in the identification and delineation of the FFA. The spatial specificity for the rest of our spatial data (precuneus/IFG/ACC) is less precise, in line with the standard spatial resolution of the MNE inverse mapping process.

Long-Range Coherence Analysis. ***FFA time course.*** To compute coherence between the FFA and each vertex on the cortex, we first averaged the MEG source waveforms across all vertices of the FFA. This yielded a mean time course for the FFA, which was used as the seed in computations of coherence with the rest of the cortical vertices. To avoid signal cancellation, the averaging took into account the polarity mismatches that occur because of MNE estimate spreading across sources whose orientations were not aligned. This was done by flipping the polarity of the signals from sources that were oriented at greater than 90° relative to a principal direction of the cortical normals within the FFA region.

Coherence computation. We computed the coherence between the averaged time course across the FFA and every other vertex on the cortex, from 6 Hz to 55 Hz, for each participant. Coherence computations were carried out on single trials and performed in MATLAB using the FieldTrip toolbox (29). For each condition, coherence was computed using a moving time window, from 800 ms before stimulus onset to 1,200 ms after stimulus onset. This procedure allowed us to compute long-range coherence in space as well as in time. The window length was seven cycles, and thus inversely proportional to the frequency. The results from each frequency were binned by frequency band and averaged within each band to obtain a mean band coherence value for each point in time for each vertex, condition, and participant. For alpha, the only frequency band in which we found significant group differences, results ranging from 8–12 Hz were averaged.

Z-Coherence. We eliminated the statistical bias due to the non-Gaussian distribution of coherence values and unequal sample sizes, as well as the problem of spurious coherence (30), by using Z-Coherence (31), a normalized coherence measure in which the principal condition (emotional faces, a total of 80 trials per participant) is normalized with respect to a baseline condition (houses, a total of 40 trials per participant). The Z-Coherence is defined as:

$$\text{Z—Coherence} = \frac{\left(\tanh^{-1}(\| C_1(f) \|) - \left(1/(N_1-2)\right)\right) - \left(\tanh^{-1}(\| C_2(f) \|) - \left(1/(N_2-2)\right)\right)}{\sqrt{(1/(N_1-2)) + (1/(N_2-2))}},$$

where N_1 and N_2 denote the degrees of freedom in the first and second conditions, respectively; C_1 is coherence in the principal condition (emotional faces); and C_2 is coherence in the baseline condition (houses). The sign of this quantity indicates whether coherence in the principal condition is higher (positive) or lower (negative) than in the baseline condition. Z-Coherence was computed for individual cortical surfaces, and the results were then morphed onto the FsAverage cortex surface using the morphing maps provided by the MNE tools. Fig. S9 outlines this procedure in detail.

Local PAC Analysis. PAC between the alpha band phase and gamma band amplitude was quantified for each vertex in the FFA, for each participant, using the modulation index (MI), which is a statistical score representing the degree of coupling between two time series, one of phase and the other of amplitude (32). This procedure was modified for epoched data by computing PAC as measured by the MI between the frequencies of 7 Hz and 13 Hz for phase and between the frequencies of 40 Hz and 130 Hz for amplitude for each single trial (epoch) and then computing the median across all epochs within a condition. It was also modified for computing alpha, rather than theta, phase coupling by setting amplitude series filter bandwidths to 12 Hz. For the baseline, each epoch lasted from 900 ms before stimulus onset to 0 ms (stimulus onset). For each of the stimulus conditions, each epoch lasted from 0 ms (stimulus onset) to 1,100 ms after stimulus onset. Thus, on average, the baseline epoch spanned 9 cycles of alpha, whereas the epochs for each of the conditions spanned 11 cycles of alpha.

To normalize PAC values in the same way that we normalized coherence values, we defined Z-PAC as the PAC due to a principal condition (emotional faces, 80 trials per participant) normalized with respect to a baseline condition (houses, 40 trials per participant). We computed Z-PAC by performing the Wilcoxon rank-sum test, which allows for an unequal number of trials, between the principal condition (emotional faces) and the baseline condition (houses), using single trials. The rank-sum test, in addition to a P value, also gives as an outcome a Z-value that quantifies the difference between the two conditions. We refer to this rank-sum Z-value as the Z-PAC. Fig. S10 outlines this procedure.

For the global PAC plot (Fig. 3*C* and Figs. S2 and S3), we repeated this procedure for every voxel in the cortex; however, due to computation time, we limited the analysis to PAC between the phase of alpha (8–12 Hz) and the amplitude of high gamma (75–110 Hz), where group difference was maximal.

Finally, there are multiple methods of computing PAC (33, 34). To ensure the robustness of our measurements, we computed PAC using three additional independent methods (35–37) in a subset of our participants. All these approaches yielded similar results. We chose to use the MI method of Canolty et al. (32) because it is inherently a statistical measure, and thus more amenable to generating a null hypothesis for the purpose of comparing the results across groups.

QDA. QDA is a standard classification procedure also known as Fisher discriminant analysis (38). Unlike LDA, QDA classifies data using a quadratic function. To assess the validity of the procedure, the data were split randomly 1,000 times into a training set (75% of participants) and a test set (25% of participants). For each of the 1,000 permutations, the QDA model estimated the prediction function on the training set, and the results were tested on the test set. This procedure yielded 1,000 classification results. The SE associated with the procedure was less than 0.05% for all values (sensitivity, specificity, and accuracy), which confirms the validity of the classifier.

1. Delorme A, Makeig S (2004) EEGLAB: An open source toolbox for analysis of single-trial EEG dynamics including independent component analysis. *J Neurosci Methods* 134(1):9–21.
2. Axmacher N, et al. (2010) Cross-frequency coupling supports multi-item working memory in the human hippocampus. *Proc Natl Acad Sci USA* 107(7):3228–3233.
3. Wolff JJ, et al. (2012) Differences in white matter fiber tract development present from 6 to 24 months in infants with autism. *Am J Psychiatry* 169(6):589–600.
4. Lord C, Rutter M, DiLavore PC, Risi S (1999) *Autism Diagnostic Observation Schedule—WPS (ADOS-WPS)* (Western Psychological Services, Los Angeles).
5. Kaufman AS, Kaufman NL (2004) *Kaufman Brief Intelligence Test* (AGS Publishing, Circle Pines, MN), 2nd Ed.
6. Piro JM (1998) Handedness and intelligence: Patterns of hand preference in gifted and nongifted children. *Dev Neuropsychol* 14:619–630.
7. Lundqvist D, Flykt A, Öhman A (1998) The Karolinska Directed Emotional Faces - KDEF, CD ROM from Department of Clinical Neuroscience, Psychology section, Karolinska Institutet, ISBN 91-630-7164-9.
8. Gur RC, Sara R, Hagendoorn M, et al. (2002) A method for obtaining 3-dimensional facial expressions and its standardization for use in neurocognitive studies. *J Neurosci Methods* 115:137–143.
9. Brainard DH (1997) The Psychophysics Toolbox. *Spatial Vision* 10:433–436.
10. Pelli DG (1997) The VideoToolbox software for visual psychophysics: Transforming numbers into movies. *Spatial Vision* 10:437–442.
11. Dale AM, Fischl B, Sereno MI (1999) Cortical surface-based analysis. I. Segmentation and surface reconstruction. *Neuroimage* 9(2):179–194.
12. Fischl B, Sereno MI, Dale AM (1999) Cortical surface-based analysis. II: Inflation, flattening, and a surface-based coordinate system. *Neuroimage* 9(2):195–207.
13. Cheour M, et al. (2004) Magnetoencephalography is feasible for infant assessment of auditory discrimination. *Exp Neurol* 190(Suppl 1):S44–S51.
14. Taulu S, Simola J (2006) Spatiotemporal signal space separation method for rejecting nearby interference in MEG measurements. *Phys Med Biol* 51(7):1759–1768.
15. Taulu S, Kajola M, Simola J (2004) Suppression of interference and artifacts by the Signal Space Separation Method. *Brain Topogr* 16(4):269–275.
16. Vidaurre C, Sander TH, Schlögl A (2011) BioSig: The free and open source software library for biomedical signal processing. *Comput Intell Neurosci* 2011:935364.
17. Klin A, Jones W, Schultz R, Volkmar F, Cohen D (2002) Visual fixation patterns during viewing of naturalistic social situations as predictors of social competence in individuals with autism. *Arch Gen Psychiatry* 59(9):809–816.
18. Pierce K, Müller RA, Ambrose J, Allen G, Courchesne E (2001) Face processing occurs outside the fusiform 'face area' in autism: Evidence from functional MRI. *Brain* 124(Pt 10):2059–2073.
19. Bailey AJ, Braeutigam S, Jousmäki V, Swithenby SJ (2005) Abnormal activation of face processing systems at early and intermediate latency in individuals with autism spectrum disorder: A magnetoencephalographic study. *Eur J Neurosci* 21(9):2575–2585.
20. Dalton KM, et al. (2005) Gaze fixation and the neural circuitry of face processing in autism. *Nat Neurosci* 8(4):519–526.
21. Hadjikhani N, et al. (2004) Activation of the fusiform gyrus when individuals with autism spectrum disorder view faces. *Neuroimage* 22(3):1141–1150.
22. Perlman SB, Hudac CM, Pegors T, Minshew NJ, Pelphrey KA (2011) Experimental manipulation of face-evoked activity in the fusiform gyrus of individuals with autism. *Soc Neurosci* 6(1):22–30.
23. Hämäläinen MS, Sarvas J (1989) Realistic conductivity geometry model of the human head for interpretation of neuromagnetic data. *IEEE Trans Biomed Eng* 36(2):165–171.
24. Dale AM, et al. (2000) Dynamic statistical parametric mapping: Combining fMRI and MEG for high-resolution imaging of cortical activity. *Neuron* 26(1):55–67.
25. Lin FH, et al. (2006) Assessing and improving the spatial accuracy in MEG source localization by depth-weighted minimum-norm estimates. *Neuroimage* 31(1):160–171.
26. Fischl B, Sereno MI, Tootell RB, Dale AM (1999) High-resolution intersubject averaging and a coordinate system for the cortical surface. *Hum Brain Mapp* 8(4):272–284.
27. Gramfort A, Keriven R, Clerc M (2010) Graph-based variability estimation in single-trial event-related neural responses. *IEEE Trans Biomed Eng* 57(5):1051–1061.
28. Kanwisher N, McDermott J, Chun MM (1997) The fusiform face area: A module in human extrastriate cortex specialized for face perception. *J Neurosci* 17(11): 4302–4311.
29. Oostenveld R, Fries P, Maris E, Schoffelen JM (2011) FieldTrip: Open source software for advanced analysis of MEG, EEG, and invasive electrophysiological data. *Comput Intell Neurosci* 2011:156869.
30. Sekihara K, Owen JP, Trisno S, Nagarajan SS (2011) Removal of spurious coherence in MEG source-space coherence analysis. *IEEE Trans Biomed Eng* 58(11):3121–3129.
31. Maris E, Schoffelen JM, Fries P (2007) Nonparametric statistical testing of coherence differences. *J Neurosci Methods* 163(1):161–175.
32. Canolty RT, et al. (2006) High gamma power is phase-locked to theta oscillations in human neocortex. *Science* 313(5793):1626–1628.
33. Tort AB, Komorowski R, Eichenbaum H, Kopell N (2010) Measuring phase-amplitude coupling between neuronal oscillations of different frequencies. *J Neurophysiol* 104(2):1195–1210.
34. Penny WD, Duzel E, Miller KJ, Ojemann JG (2008) Testing for nested oscillation. *J Neurosci Methods* 174(1):50–61.
35. Tort AB, Komorowski RW, Manns JR, Kopell NJ, Eichenbaum H (2009) Theta-gamma coupling increases during the learning of item-context associations. *Proc Natl Acad Sci USA* 106(49):20942–20947.
36. Cohen MX, et al. (2009) Good vibrations: Cross-frequency coupling in the human nucleus accumbens during reward processing. *J Cogn Neurosci* 21(5):875–889.
37. Osipova D, Hermes D, Jensen O (2008) Gamma power is phase-locked to posterior alpha activity. *PLoS ONE* 3(12):e3990.
38. Pedregosa F, Varoquaux G, Gramfort A, Michel V, Thirion B (2011) Scikit-learn: Machine Learning in Python. *J Mach Learn Res* 12:2825–2830.

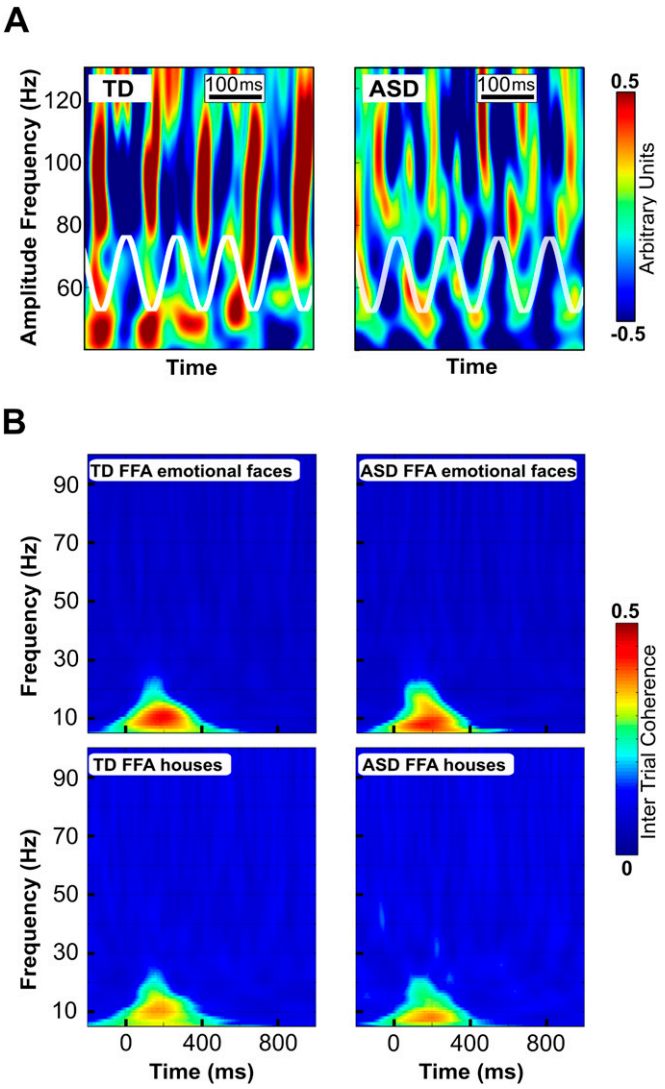

Fig. S1. (*A*) Examples of PAC from one TD participant (*Left*) and one participant with ASD (*Right*). The white sine wave shows four cycles of a 10-Hz alpha rhythm. PAC measures the extent to which the gamma power is modulated in phase with the alpha oscillations. This figure was obtained by averaging the response with respect to the trough of the alpha cycle. In the TD participant, it is clear that gamma peaks, especially high gamma peaks (~75–110 Hz) reliably coincide with the troughs of the alpha cycles. In the participant with ASD, the timing of gamma bursts is not as time-locked to the alpha troughs as in the TD participant. (*B*) Intertrial coherence (ITC), which measures the consistency of phase across trials, was computed using the standard approach. We calculated a continuous time-frequency decomposition using seven-cycle Morlet wavelets for each trial and then computed the phase in each trial continuously. ITC is then defined as the mean vector length on unit circles across trials. We did not find any group differences in ITC in the FFA in either the houses or emotional faces conditions.

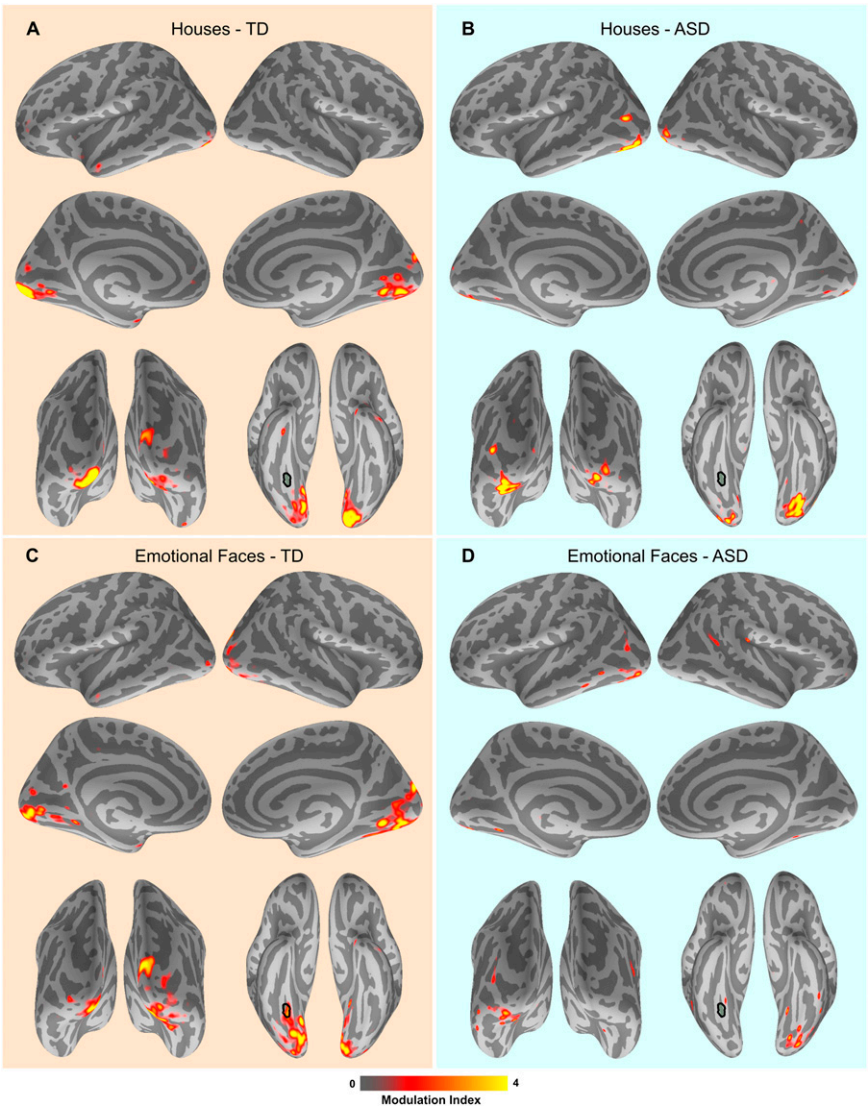

Fig. S2. Whole-cortex alpha to high gamma PAC analysis for houses and emotional faces conditions computed at the frequencies corresponding to the maximum contrast (alpha phase to high gamma: 75–110 Hz amplitude; Fig. 3). The four views of the cortex presented in each panel are used to display PAC (significant PAC is represented by higher, colored MI values) over the entire cortex. (*A*) Average PAC for the TD group during the houses condition. There was significant PAC in the occipital cortex only and none within the FFA, shown outlined in bold on the ventral view. (*B*) Average PAC for the ASD group during the houses condition. As in the TD group, there is no significant alpha to high gamma PAC in the FFA (bold outline.) (*C*) Average PAC for the TD group during the emotional faces condition. Here, there is significant PAC in the FFA (bold outline). (*D*) Average PAC for the ASD group during the emotional faces condition. Unlike the TD group, there is no significant PAC in the FFA (bold outline).

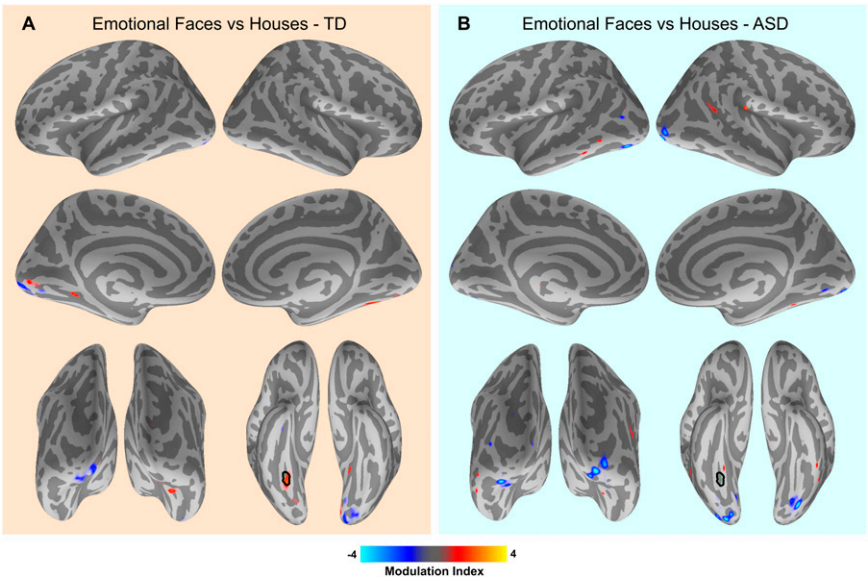

Fig. S3. PAC for the emotional faces condition normalized by PAC for the houses condition (Z-PAC) over the whole cortex. The ventral view shown here is also presented in Fig. 3*C*. (*A*) Normalized PAC (i.e., data shown in Fig. S2*C* normalized by data shown in Fig. S2*A*) for the TD group. The largest area of significant positive normalized PAC (i.e., PAC greater for emotional faces than for houses) is within the FFA, outlined in bold in the ventral view. (*B*) Normalized PAC (i.e., data shown in Fig. S2*D* normalized by data shown in Fig. S2*B*) for the ASD group. There is no increase in PAC for emotional faces over houses within the FFA. Several small areas in the occipital lobe show increased PAC for houses over faces.

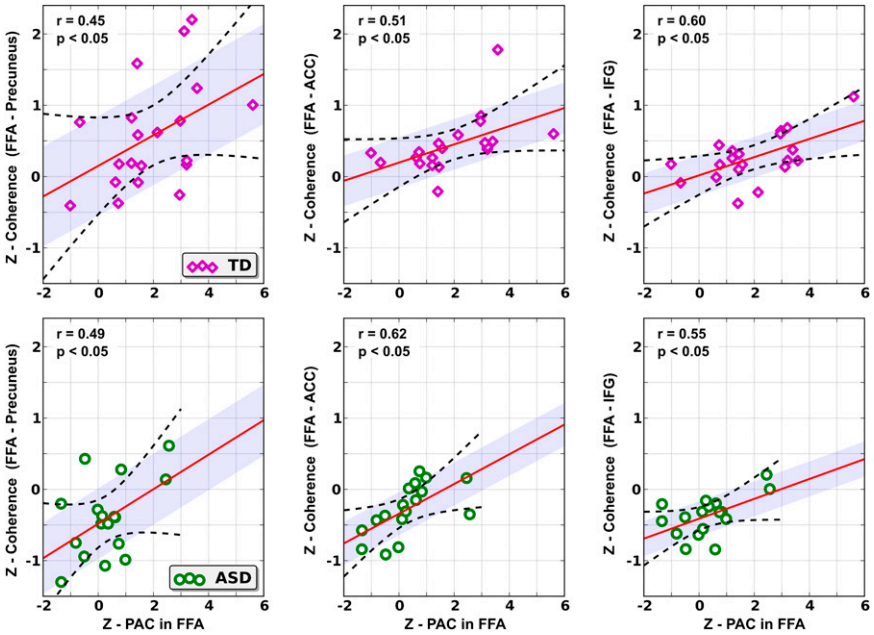

Fig. S4. Correlation between Z-PAC and Z-Coherence is the same as in Fig. 4, but with data plotted separately for each group. Correlations between the magnitude of Z-PAC and the magnitude of Z-Coherence remain significant within each group for all three regions of interest (precuneus, ACC, and IFG).

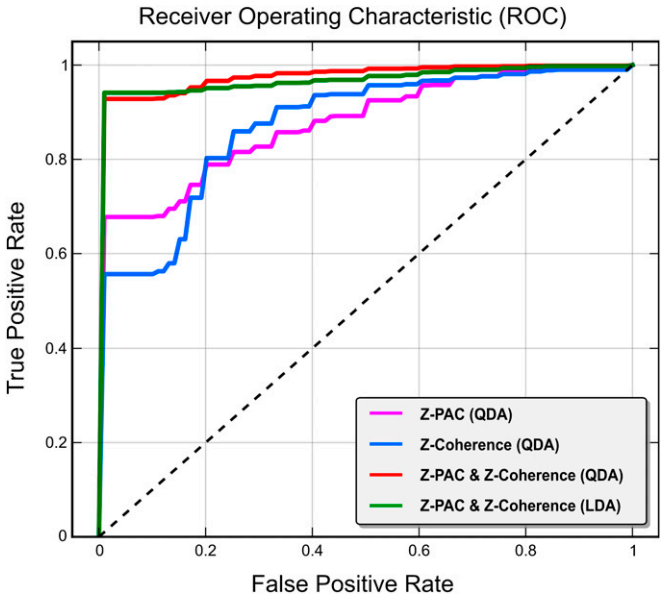

Fig. S5. ROCs showing performance of statistical classifiers using different subsets of features and different approaches. For each case, we evaluated the performance of the classifier using the standard approach of measuring the area under the curve (AUC), where an AUC of 0.5 represents chance (dashed line). Magenta, QDA classifier when only Z-PAC data were used (AUC = 0.876); blue, QDA classifier when only Z-Coherence data were used (AUC = 0.872); red, QDA classifier using both Z-PAC and Z-Coherence data (AUC = 0.974); green, LDA classifier using both Z-PAC and Z-Coherence data (AUC = 0.967). The performance of the QDA classifier significantly improved when both Z-PAC and Z-Coherence data were used. The performance of the LDA classifier was similar to that of the QDA classifier.

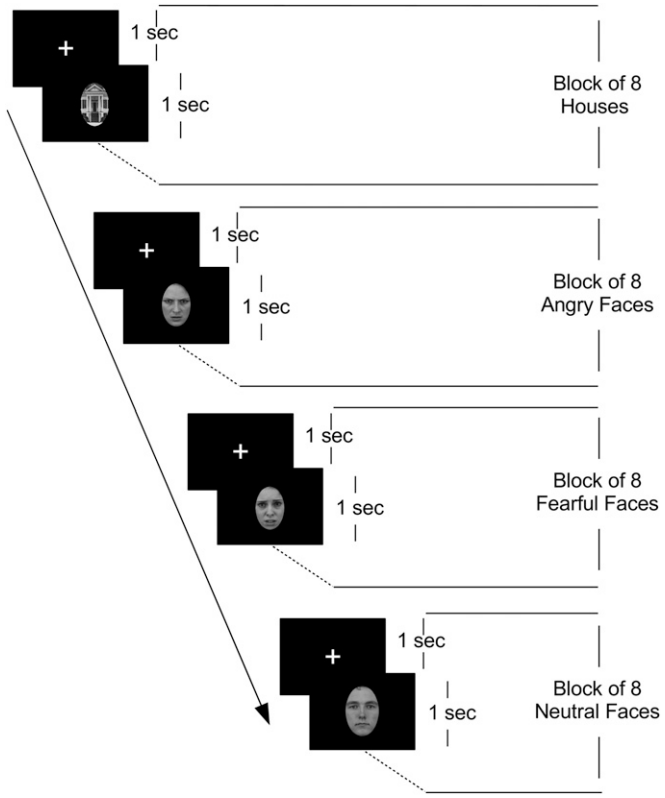

Fig. S6. Experimental paradigm. We had three runs in total. Each run consisted of two blocks, with each containing 8 stimuli from the same condition, for a total of 48 distinct stimuli per condition.

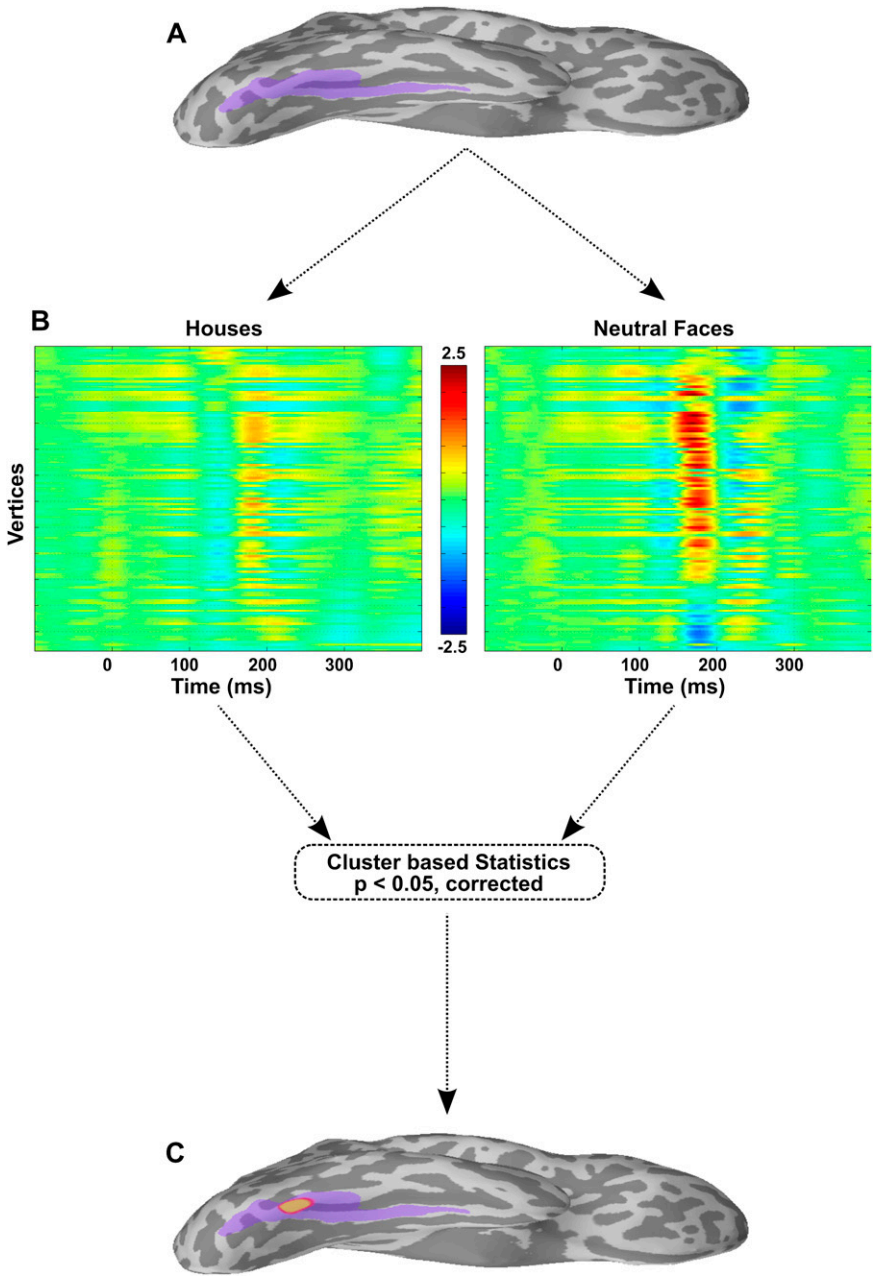

Fig. S7. Delineating the FFA. (*A*) For each participant, we extracted single-trial data corresponding to the FreeSurfer fusiform gyrus (FG) label. (*B*) These trials were then aligned in time (the averages are shown) and subjected to cluster-based statistics ($P < 0.05$ corrected) to determine which cluster of vertices within the FG responded significantly more to neutral faces than to houses over the duration of each trial. (*C*) This cluster was then delineated as the FFA for that participant.

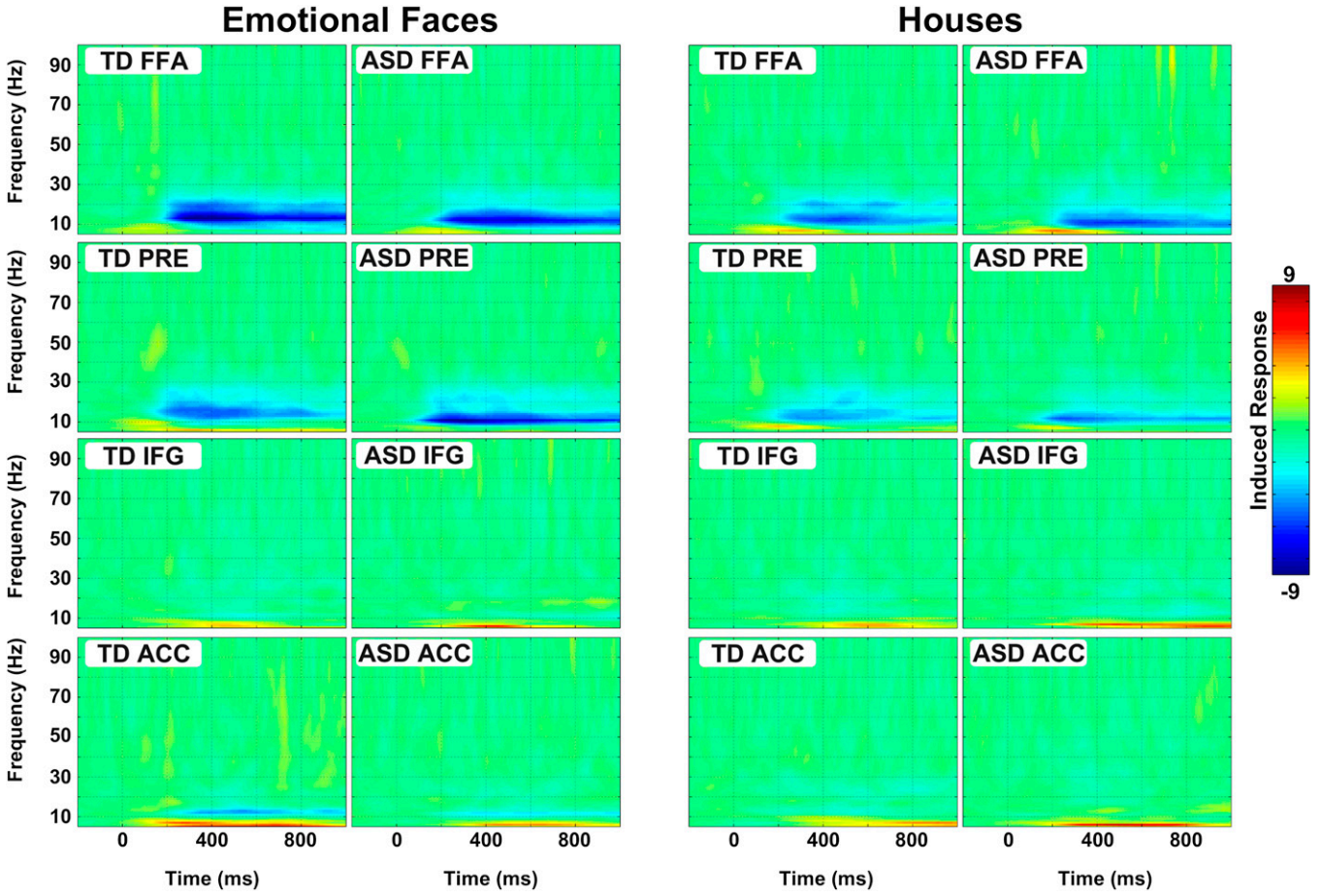

Fig. S8. Induced response in the FFA, precuneus, IFG, and ACC for each group in the emotional faces (*Left*) and houses (*Right*) conditions. The induced response was calculated by first subtracting the evoked response from each trial, followed by time-frequency decomposition using seven-cycle Morlet wavelets. Using the mean and SD in the baseline time window (−350 to −10 ms), we computed the Z-score for each trial as a function of time and frequency; the induced response was defined as the mean Z-score value across all trials. After correcting for multiple comparisons using cluster-based statistics, we found no significant group differences in induced responses in any of the conditions or areas.

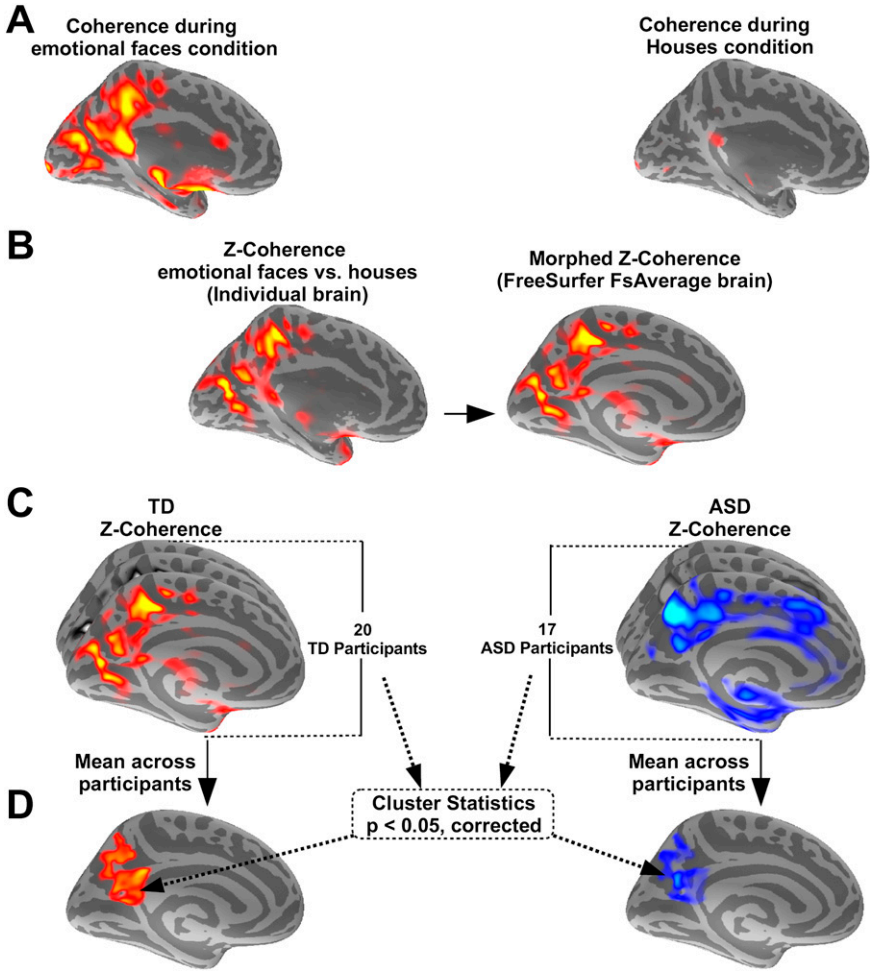

Fig. S9. Computation of Z-Coherence group differences. (*A*) Event-related coherence between the FFA and the rest of the cortex was computed using a moving time window, for each participant (one example from the TD group shown) for the emotional faces (*Left*) and houses (*Right*) conditions. Shown here is a single time snapshot, from $t = 150$ ms after stimulus onset. (*B*) Z-Coherence was computed for each participant and morphed from the individual brain (*Left*) to the FsAverage brain (*Right*). (*C*) This procedure was repeated for each participant. (*D*) Mean group Z-Coherence value at $t = 150$ ms, masked at significant group difference (i.e., all Z-Coherence values outside the significant cluster were set to 0) ($P < 0.05$ corrected).

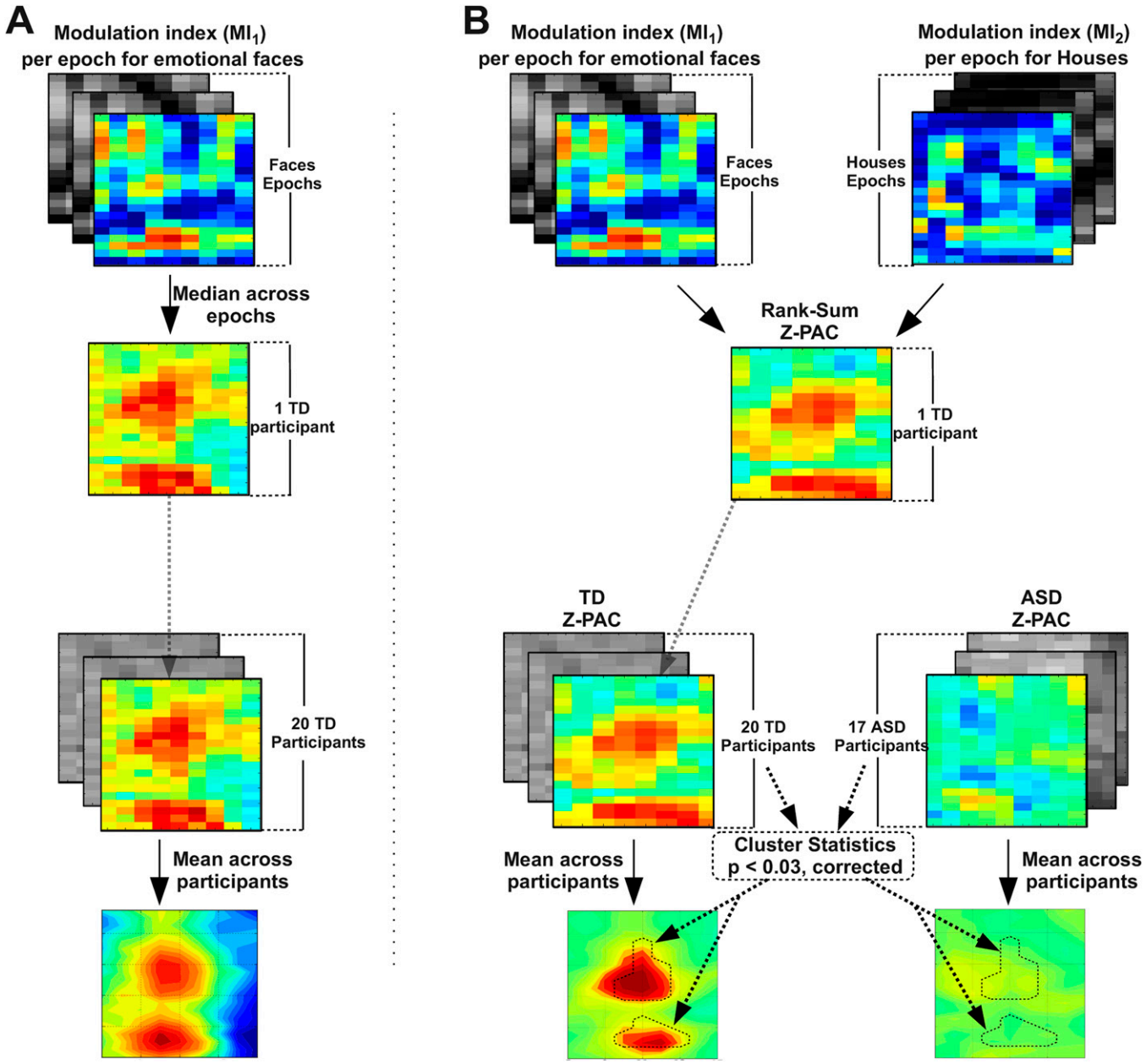

Fig. S10. Computation of Z-PAC group differences. (*A*) (*Top*) MI in the FFA was computed for each participant for individual trials in each condition. (*Upper Middle*) Median across trials was computed for each participant and condition. We used the median rather than the mean because (*i*) the MI is always positive and the values are not normally distributed, (*ii*) the median is less susceptible to noise, and (*iii*) the median is a more natural value for the rank-sum test than the mean. (*Lower Middle*) We repeated this procedure for each participant. (*Bottom*) We took the mean across participants, and the result was the corresponding (group, condition) panel in Fig. 3*A*. (*B*) (*Top Left*) Same as *Top* in *A*. (*Top Right*) Same as *Top* in *A*, for the houses condition. (*Upper Middle*) Z-PAC (PAC for emotional faces normalized by PAC for houses) was then computed for that participant. (*Lower Middle*) Procedure was repeated for each participant. (*Bottom*) Cluster-based statistics were used to determine regions of significant group differences. Dashed line marks areas that showed significant group difference ($P < 0.03$ corrected) overlaid on the mean Z-PAC plot for each group (as in Fig. 3*B*).

Table S1. Participant data

	ASD (n = 17), mean (SD), range	TD (n = 20), mean (SD), range	t (35), P value
Age, y	16.8 (2.0), 14–20	16.5 (2.5), 13–21	0.4, 0.67
SCQ lifetime	22.0 (3.8), 16–28	3.4 (3.8), 1–15	14.4, 0.000
ADOS communication	3.4 (1.7), 1–7	—	—
ADOS social	7.6 (2.6), 4–12	—	—
Verbal IQ	112 (21), 61–142	115 (10), 93–132	0.6, 0.56
Nonverbal IQ	112 (16), 74–132	112 (18), 74–132	0.1, 0.92

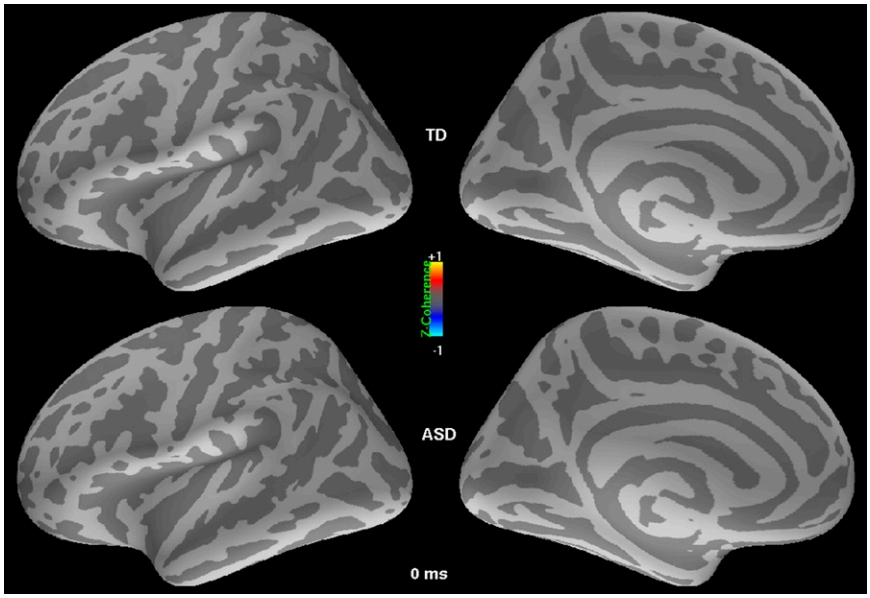

Movie S1. Z-coherence (coherence during viewing of emotional faces normalized by coherence during viewing of houses) as a function of time relative to stimulus onset. The TD group (*Upper*) and the ASD group (*Lower*) are shown.

Movie S1

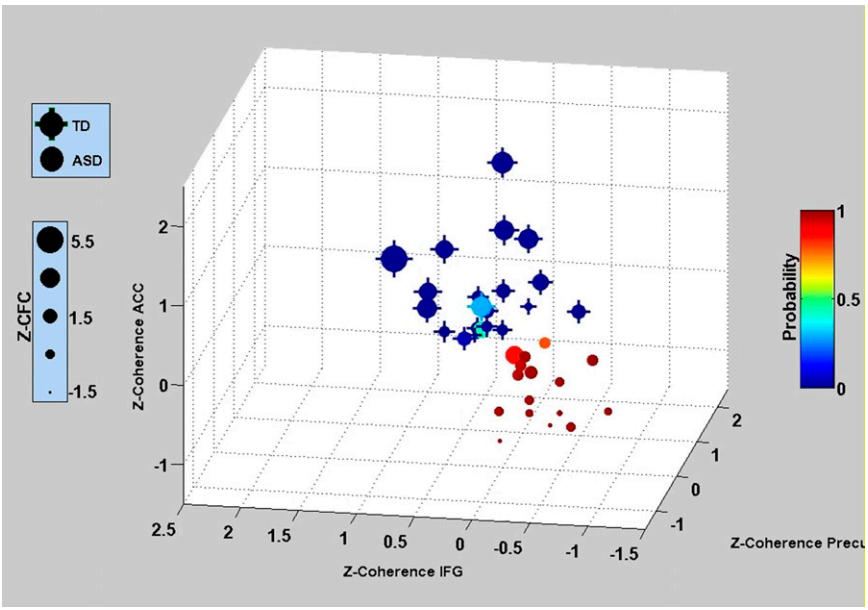

Movie S2. Rotating visualization of the 5D depiction of the QDA shown in Fig. 5*B*: the three Z-Coherence values for the precuneus, ACC, and IFG (the three axes); Z-PAC (size of the marker); and probability of that participant having an ASD diagnosis (color of the marker). Plain circles represent participants with ASD, and crossed circles represent TD participants. For all but 1 of the 37 participants, the probability of having an ASD diagnosis is assigned correctly (i.e., greater than or less than 50% in agreement with the actual diagnosis). Only 1 participant with ASD is assigned an ambiguous probability of about 50% for carrying an ASD diagnosis. The movie clearly shows that a hypercurve exists that will correctly separate ASD participants from TD participants for all but 1 participant.

Movie S2